The Control of Laminar Separation Bubbles Using High- and Low-Amplitude Forcing

Mark Phil Simens[1] and Javier Jiménez[1,2]
School of Aeronautics, Universidad Politécnica de Madrid, 28040 Madrid, Spain; E-mail: mark@torroja.dmt.upm.es
[2]*Center for Turbulence Research, Stanford University, Stanford, CA 94305-3035, U.S.A.*

Abstract. Two-dimensional simulations are used to demonstrate the existence of two different amplitude regimes to control laminar separation bubbles with periodic zero-mass-flux wall jets. One is based primarily on a shear-layer instability found using low-amplitude forcing. The minimum bubble length is obtained for a Strouhal number approximately equal to 0.018, based on a properly defined momentum thickness. Higher forcing is found to create large vortices, which are responsible for very effective control. A relation is presented between the forcing parameters and the size of the vortices. These estimates are then used to explain the range of effective frequencies to control the separation bubble.

Key words: Strong forcing, Kelvin–Helmholtz, instability, vortex shedding, separated flow, boundary layers, control.

1 Introduction

Separation is an important problem in aviation and in turbo-machinery, which can in part be remedied using passive or active control. A lot of work has been done on active control of separation bubbles and a good overview can be found in [8]. Two other works should be highlighted. It is postulated in [5] that the forcing excites the shear layer formed by the separation bubble in such a way that big shed vortices are formed. It is found in [2] that, at high forcing amplitudes and at certain frequencies, the bubble is absent.

Here we describe the active control of laminar two-dimensional separation bubbles using periodic-zero-mass-flux wall jets. Results for a wide range of pressure gradients, forcing frequencies and forcing amplitudes will be discussed. Finally, a simple model is proposed to explain the results for strong forcing (10% of the free stream velocity).

J.F. Morrison et al. (eds.), IUTAM Symposium on Flow Control and MEMS, 191–197.

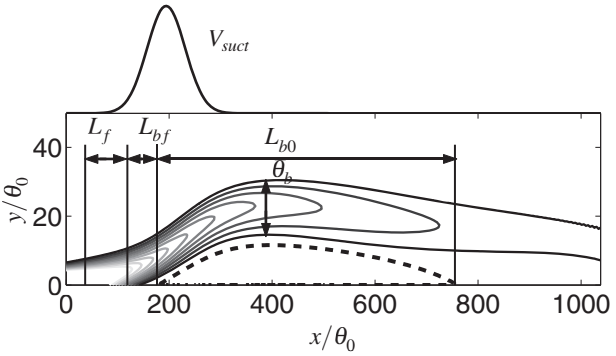

Fig. 1 The numerical domain used throughout the study. – – – – : initial separation bubble. ——— : ω_z contours given by $-0.12{:}0.03{:}-0.03\ U_\infty/\theta_0$.

1.1 Numerical Techniques and Unperturbed Flows

The Navier–Stokes equations are discretized using second-order central finite difference schemes on a staggered grid. Time integration is done using a low-storage third-order Runge–Kutta scheme [7] for the convective terms, while the viscous terms are treated implicitly. A fractional-step method based on [9] is employed to assure the conservation of mass, and to obtain the pressure in an efficient manner.

The numerical simulations have been done in two dimensions over a flat plate (Figure 1). At the inlet, the streamwise component, u, of the Blasius profile is imposed, while the component perpendicular to the wall, v, is imposed to be zero. No-slip boundary conditions are imposed at the bottom wall, while impermeability is assumed for v along most of the bottom wall. The exception is a small segment in which a periodic zero-mass-flux forcing is imposed, given by $v(x, y = 0, t) = V_f \sin(2\pi f t)$. The u velocity at the upper wall is modeled using a vorticity-free condition $\partial_y u(x, y = L_y, t) = \partial_x v(x, y = L_y, t)$. Adverse pressure gradients are obtained by imposing a suction profile $V_{suct}(x, y = L_y, t) = a_s \exp(-b_s(x - c_s)^2)$, similar to that used in [1].

In the case of arbitrary mass fluxes over the boundaries, a modification of the standard procedure was necessary to guarantee global mass conservation. It consists in expressing the total solution for the correction of the pressure $\phi_{tot} = \phi_1 + C(x^2 - y^2)$ as the sum of the solution ϕ_1 of the Poisson equation, and a function satisfying the Laplace equation $C(x^2 - y^2)$. The Poisson equation for ϕ_1, singular due to Neumann boundary conditions, is solved with the aid of cosine Fourier decomposition. A solution can only be obtained when the zero mode $k = 0$, $\widehat{\phi}_1(k = 0, L_y) = 0$ is imposed. However, if the total mass flow through the boundaries is not zero, the derivative $\partial\widehat{\phi}(k = 0, L_y)/\partial n \neq 0$. The constant C is used to force $\partial\widehat{\phi}(k = 0, L_y)/\partial n = 0$, creating a pressure gradient that assures the correct mass flow, allowing $\partial\widehat{\phi}/\partial n \neq 0$ at the exit. The outflow boundary conditions then become $\partial_t \mathbf{u}_{x=L_x,y,t} + U_\infty \partial_x \mathbf{u}_{x=L_x,y,t} + \partial_x \phi_{\mathrm{tot}}|_{x=L_x,y,t} = 0$.

The Reynolds number of most simulations, based on the inlet momentum thickness θ_0, is $Re_{\theta_0} = 30$, while at separation it is $Re_{\theta_s} \approx 110$. For comparison a few other cases were run at higher Reynolds numbers. The length of the numerical domain, adimensionalized with θ_0, is $L_x \times L_y = 1047 \times 133$, and is discretized using $N_x \times N_y = 256 \times 128$ points. The time step is determined using a constant CFL $= 0.6$. At $Re_{\theta_0} = 30$, all the separation bubbles were stable and reattached due to viscous diffusion.

2 Low-Amplitude Forcing

The low-amplitude forcing is expected to trigger the instability of the shear layer formed by separation. This necessarily would imply that the most unstable frequency lies around $St_\theta = f\theta_b/U_\infty = 0.018$ [11], which has been obtained for separated flow in [6]. Here the momentum thickness θ_b has been measured at the position of maximum negative velocity inside the bubble. It was proposed in [10] that triggering shear layer instabilities could be useful in reducing the separation bubble, but they did not scale their results with a suitable momentum thickness. Instead, they used the length of the initial separation bubble, L_b, if the flow reattaches before the trailing edge; in the case where the flow stalls, the length of the airfoil is used. This results in a most unstable frequency of around $St_F = fL_b/U_\infty \approx 1$.

In Figure 2, the most effective Strouhal number as a function of the minimum bubble length are shown. The two different scalings based on θ_b (Figure 2a), and L_b (Figure 2b) have been used. One observes that the scaling based on θ_b gives much better collapse than the one based on the initial length of the separation bubble. The results, when scaled with θ_b, tend to an asymptotic value for long bubbles. The deviation from 0.018 is presumably due to the presence of the wall, and to the shear layer not being parallel.

The physical reasoning behind $St_F \approx 1$ was discussed in [8], still in terms of the shear layer instability. Recently however, the same group [3] related $St_F \approx 1$ to stalled flow in which the important length scales are the wake width and the wavelength of the periodic vortex roll-up. This is different from the flow under consideration here. To explain the different scaling laws obtained by both groups, we propose to make a distinction between stalled flows, and closed separation bubbles. In the latter, the most effective frequency would be $St_\theta \approx 0.018$, and in the former $St_F \approx 1$ may be appropriate.

3 High-Amplitude Forcing

High-amplitude forcing creates an instantaneous separation bubble that rolls-up to form a large vortex. This vortex is very effective in controlling the separation, because it forms upstream of the bubble. The roll-up is difficult to describe in detail,

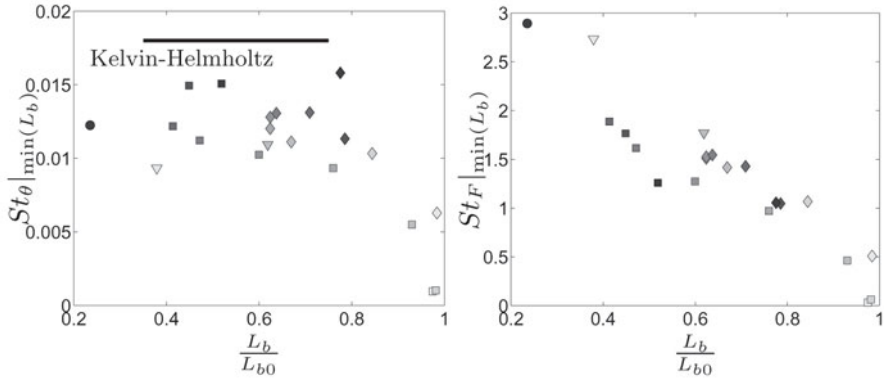

Fig. 2 (a) Scaling of the optimum frequency with θ_b and (b) with L_{b0}. With $c_s/L_x \approx 0.19$: ■ : $Re_{\theta_0} = 30$; ▼ : $Re_{\theta_0} = 100$, with $L_x/\theta_0 \times L_y/\theta_0 \approx 785 \times 84$ and $N_x = 512$, $N_y = 128$; • : $Re_{\theta_0} = 21$, with $L_x/\theta_0 \times L_y/\theta_0 \approx 2094 \times 133$ and $N_x = 512$, $N_y = 128$ ♦ : $Re_{\theta_0} = 30$, $c_s/L_x \approx 0.38$. In all cases, $V_f/U_\infty = 0.001$. Gray indicates short bubbles, black long bubbles.

but the principal idea is that the vortex size is determined by the mass entrained. The characteristic thickness at forcing is approximated by θ_b. The area of the vortex is given by $\pi r^2 = t_s U_\infty \theta_b$, where $t_s U_\infty \theta_b$ is the fluid the vortex entrains during a time t_s. A second length scale D, defined to first order as the shear layer lift-up V_f/f, determines the shedding frequency, $f_s D/U_\infty \sim 0.2$, assuming that the process is similar to the vortex shedding behind an obstacle. Substituting $t_s = 1/f_s$ in r gives

$$\frac{r}{\theta_b} \sim \sqrt{5\frac{V_f}{\pi f \theta_b}}. \tag{1}$$

A different estimation for the radius was derived in [4] by assuming that the vortex entrains all the mass added during the blowing phase of the forcing, but we now believe that the present estimate is more accurate.

The radius in Equation (1) is used to approximate the circulation $\Gamma = \int \omega dA$, with constant $\omega = U_\infty/\theta_b$ and $A = \pi r^2$. This, at time t_s, results in

$$\frac{\Gamma}{U_\infty \theta_b} = \frac{5V_f}{f\theta_b}. \tag{2}$$

These estimates agree reasonably well with the results from numerical experiments (not shown), especially considering the crude approximations involved.

3.0.1 The Important Parameters for High-Amplitude Control

The correct estimation of the vortices, as a function of the forcing parameters, is only useful if it can be related to the effectiveness in controlling the separation bubble.

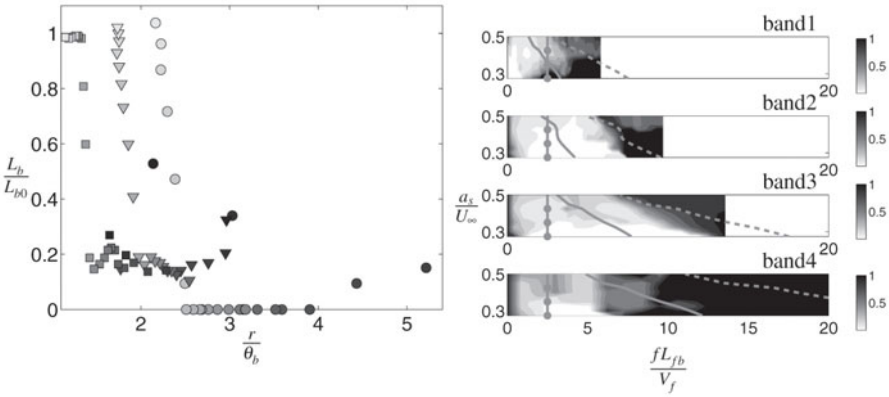

Fig. 3 (a) Relation between measured vortex radius and their effectiveness expressed in bubble reduction L_b/L_{b0}. Gray (high frequency) to black (low frequency) shading is used to distinguish between frequencies. ○ : $as/U_\infty = 0.3$, □ : $as/U_\infty = 0.375$, △ : $as/U_\infty = 0.45$. (b) The reduction in bubble length as a function of a measure of the pressure gradient and the adimensional frequency. The bubble length is indicated by shaded contours with levels given by (0:0.1:1). ——●—— : $fL_{fb}/V_f = 2.5$; - - - - : $fL_{fb}/V_f = 20L_{fb}/25\pi\theta_b$. ——— : $0.018\frac{U_\infty L_{fb}}{V_f\theta_b}$. From top to bottom: $L_{fb}/\theta_0 \approx 62,\ 103,\ 144,\ 226$.

We will make two assumptions to obtain this relation. The first one is that the vortex should form before it reaches the separation bubble to be effective. The time that the forming vortex needs to get to the separation bubble is L_{fb}/U_c, where $U_c \approx U_\infty/2$ is the convective velocity of the vortex. This should be larger than the time t_s that the vortex needs to form, giving

$$\frac{L_{fb}}{U_c} \geq \frac{5V_f}{fU_\infty}, \quad \text{or} \quad \frac{fL_{fb}}{V_f} \geq 5\frac{U_c}{U_\infty} \sim 2.5. \tag{3}$$

The second assumption is that the radius of the vortex r/θ_b is larger than some number, which is fitted empirically to 2.5 from Figure 3a. Only then it can effectively mix fluid from the separation zone with the free stream. Using the estimation (1), this gives

$$\frac{f\theta_b}{V_f} \leq \frac{25\pi}{20}, \quad \text{and after multiplying by} \quad \frac{L_{fb}}{\theta_b}, \quad \text{gives} \quad \frac{fL_{fb}}{V_f} \leq \frac{20L_{fb}}{25\pi\theta_b}. \tag{4}$$

The assumption leading to Equation (4) is tested in Figure 3a, where it is seen that $2.5 \leq r/\theta_b \leq 3.5$ is required for maximum efficiency.

Figure 3b tests the limits in Equations (3) and (4), which are given by the gray circles and the dashed lines. In general the agreement is reasonable considering the approximations made. The limits effectively mark the most efficient forcing frequencies.

The failure for higher reduced frequencies, especially in band 4, is probably due to viscous effects. At higher frequencies the radius of the vortices gets smaller, and although they might be strong when formed, they get weaker due to viscous diffusion before they reach the separation bubble. The positive results obtained for band one completely outside the limits of (3) and (4) is probably related to the positive effect of suction.

4 Conclusions

Two ways to force a separated laminar boundary layer are examined. For weak intensities, the effective forcing has been shown to depend on the instability of the shear layer. The most unstable frequency scales well when adimensionalized with the appropriate momentum thickness. Adimensionalization based on the initial length of the separation bubble is less successful.

The second possibility is to create large vortices by strong forcing at a position upstream of the separation bubble. The large vortex enhances mixing along the whole APG region. The instability invoked by the weak forcing experiments causes vortices to be formed downstream of the separation point, and is therefore less effective. A rough model for the process of vortex formation gave results in satisfactory agreement with the numerical experiments. They relate the forcing parameters with the vortex size, and this in turn gives the most effective frequency range. The range also includes the Kelvin–Helmholtz instability, but this seems fortuitous, as the model is not related to an instability mechanism of the initial unperturbed separation bubble. Large vortices were also observed in [2,5], but our explanation of their formation is different from theirs. Four forcing regimes are proposed in [5], and the one related to the creation of large vortices is a shedding instability of the separation bubble, analogous with Kármán vortex shedding. Here, we also invoked a shedding type instability, but related to the instantaneous separation bubble created by the forcing.

This forcing, although more effective than triggering the instability, is more energy demanding, as higher values for the amplitude are required.

References

1. Alam, M., Sandham, N.D.: Direct numerical simulation of short laminar separation bubbles with turbulent reattachment. *J. Fluid Mech.* **410** (2000) 1–28.
2. Kiya, M., Shimizu, M., Mochizuki, O.: Sinusoidal forcing of a turbulent separation bubble. *J. Fluid Mech.* **342** (1997) 119–139.
3. Darabi, A., Wygnanski, I.J.: Active management of naturally separated flow over a solid surface. Part 1. The forced reattachment process. *J. Fluid Mech.* **510** (2004) 105–129.
4. Simens, M.P., Jiménez, J.: Alternatives to Kelvin–Helmholtz instabilities to control separation bubbles. ASME Paper GT2006-90670 (2006).

5. Sigurdson, L.W.: The structure and control of a turbulent reattaching flow. *J. Fluid Mech.* **298** (1995) 139–165.
6. Huppertz, A., Fernholz, H-H.: Active control of the turbulent flow over a swept fence. *Eur. J. of Mech. B/Fluids* **21** (2002) 429–446.
7. Spalart, P.R., Moser, R.D., Rogers, M.M.: Spectral methods for the Navier–Stokes equations with one infinite and two periodic directions. *J. Comp. Phys.* **96** (1991) 297–324.
8. Greenblatt, D., Wygnanski, I.J.: The control of flow separation by periodic excitation. *Progr. Aerospace Sci.* **36** (2000) 487–545.
9. Orlandi, P.: *Fluid Flow Phenomena*, Kluwer Academic Publisher, Dordrecht (2000).
10. Seifert, A., Pack, L.G.: Active flow separation control on wall-mounted hum at high Reynolds numbers. *AIAA J.* **40** (2002) 1363–1372.
11. Michalke, A.: On spatially growing disturbances in an inviscid shear layer. *J. Fluid Mech.* **23** (1965) 521–544.